RESEARCH ARTICLE



Check for updates

Geopolymer-based sub-ambient daytime radiative cooling coating

Ning Yang¹ | Yang Fu² | Xiao Xue³ | Dangyuan Lei² | Jian-Guo Dai¹ |

¹Department of Civil and Environmental Engineering, The Hong Kong Polytechnic University, Hung Hom, Hong Kong, China

²Department of Materials Science and Engineering, City University of Hong Kong, Kowloon Tong, Hong Kong, China ³China Southwest Architectural Design and Research Institute Co. Ltd., Chengdu, China

Correspondence

Jian-Guo Dai, Department of Civil and Environmental Engineering, The Hong Kong Polytechnic University, Hung Hom, Hong Kong, China. Email: cejgdai@polyu.edu.hk

Funding information

Research Institute for Smart Energy, The Hong Kong Polytechnic University, Grant/Award Number: CDBL; Research Institute for Sustainable Urban Development, Hong Kong Polytechnic University, Grant/Award Number: 1-BBWX; RGC General Research Fund of Hong Kong SAR, Grant/Award Number: 15223120; Hong Kong Polytechnic University; Research Institute for Sustainable Urban Development

Abstract

Sub-ambient daytime radiative cooling coating (SDRCC) is an appealing thermal management technology with great potential for alleviating the global warming and urban heat island effect. Over the past few years, various polymeric SDRCCs have been developed. However, they may face problems of environmental aging under UV and moisture due to their organic nature. In this study, an ambient-cured inorganic geopolymer-based SDRCC was synthesized with the modification of barium sulfate (BaSO₄) and nano-silica (SiO₂) particles. The optical and physicochemical properties were systematically investigated. The chemical composition, functional groups, surface morphologies of the raw materials, and the formed geopolymer coating were characterized by XRD, FTIR, SEM, and EDS. The developed coating exhibits a high infrared emissivity of 0.9491 and solar reflectance of 97.6%. When exposed to direct sunlight, the coating's surface could cool down up to 8.9 °C below the ambient air temperature under Hong Kong's climate. In addition, the coating could retain well its performance under a variety of harsh environments, including high temperature, water immersion, mechanical wearing, and exposure to sunlight.

KEYWORDS

alkali activation, daytime radiative cooling, geopolymer, sub-ambient

1 | INTRODUCTION

In the recent years, sub-ambient daytime radiative cooling (SDRC) technology has gained worldwide attention for its potential to cool the surface of an object below the ambient temperature under direct sunlight with zero energy consumption. The SDRC can be achieved by engineering a surface with a high solar reflectance as well as a high emittance in the sky transparent window (infrared atmospheric window). Specifically, the Earth is in an

Earth-Space-Sun three-body dynamic radiative heat exchange system. Assuming the Sun and Earth as black bodies, the Earth's temperature in steady state is about 279 K.¹ Actually, the average temperature of the Earth's surface is much higher than 279 K because the Earth's radiation is blocked by the Earth's surface atmosphere in most wavelength bands due to its low transmittance.² The increase in greenhouse gases in the atmosphere further blocks the outward radiation, leading to global warming and extreme climates. Fortunately, the main

This is an open access article under the terms of the Creative Commons Attribution License, which permits use, distribution and reproduction in any medium, provided the original work is properly cited.

© 2022 The Authors. EcoMat published by The Hong Kong Polytechnic University and John Wiley & Sons Australia, Ltd.

25673173, 2023, 2, Downlo

aded from https://onlinelibrary.wiley.com/doi/10.1002/eom2.12284 by City University Of Hong Kong, Wiley Online Library on [23/11/2025]. See the Terms

and-conditions) on Wiley Online Library for rules of use; OA articles are governed by the applicable Creative Commons

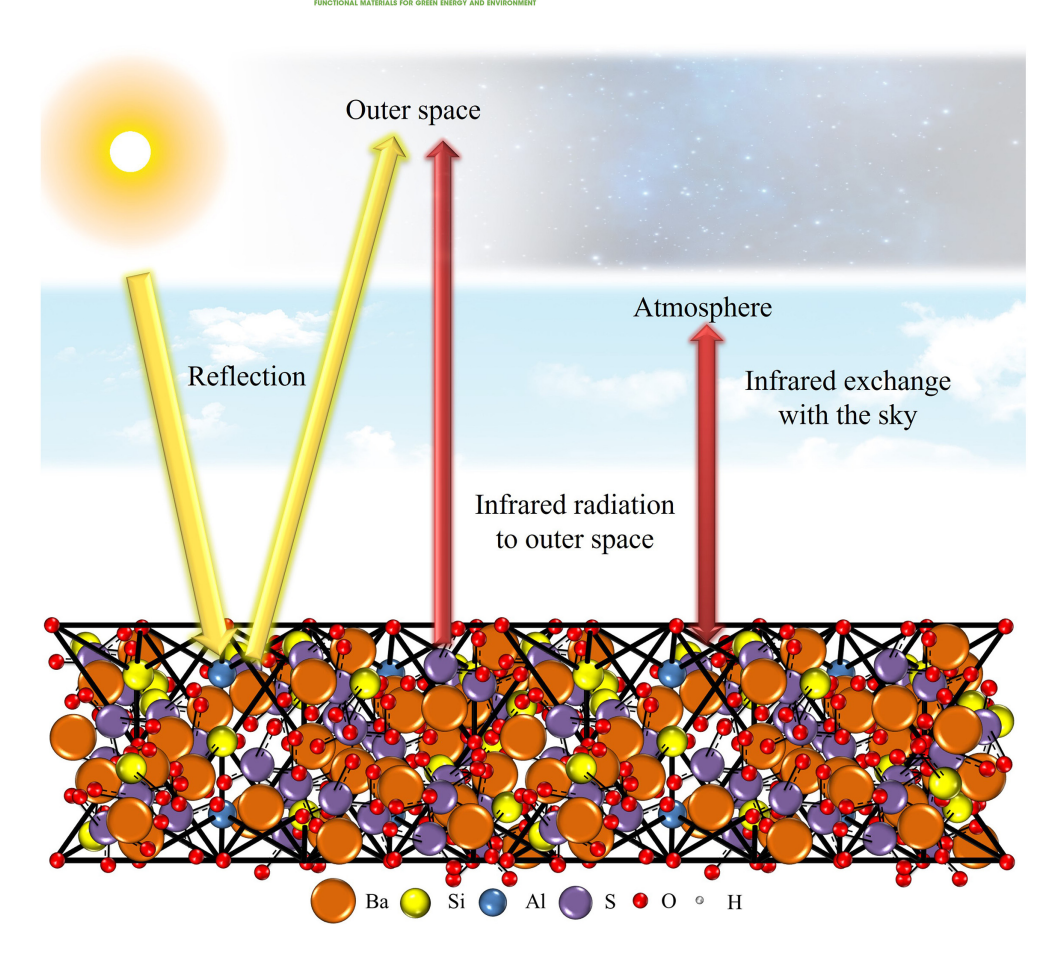


FIGURE 1 Schematic cooling mechanism of the geopolymer cooling coating

transparent band of the atmosphere, which is so-called atmospheric window, ranging from 8 to 13 µm, coincides with the peak of blackbody radiation from objects at around 300 K. Therefore, objects on the Earth can radiate heat to outer space through this "window" and be thus passively cooled down.^{3,4}

The breakthrough of SDRC technology was reported by Raman et al.,⁵ for which a sub-ambient cooling effect was achieved under direct sunlight using a planar photonic emitter. This emitter consisted of seven stacking layers of HfO₂ and SiO₂ with varying thicknesses on top of a 200-nm-thick Ag mirror and a 750-µm-thick Si substrate. A high solar reflectance of 97% and selective emission over the atmospheric window were realized. However, the above photonic structure-based technology, as well as the other metamaterials developed in the following studies, 6,7 may suffer from sophisticate micronano fabrication and the use of metallic back reflector, which high cost may impede the large-scale applications.4,6-12

Organic polymeric coatings have been then studied to promote the wider applications of SDRC technology due to their ease in manufacturing, low cost, good spectral tunability and versatile functionality (e.g., through the use of various functional fillers). 12-14 It is especially

noteworthy that many polymers are characterized with functional groups that can facilitate sufficient infrared radiation in the atmospheric window and high transparency for the solar spectrum.¹⁵ Various strategies have been adopted to enhance the cooling performance of the polymeric SDRC coatings¹⁶⁻²¹: (1) to choose organic polymer matrices with molecular bonds including C-O, C-F, C-Cl, etc., to enable high emittance in the infrared atmospheric window; (2) to further enhance the infrared radiation through phonon resonance of SiO2 microparticles; (3) to improve the solar reflectance through introducing functional fillers (TiO2, Al2O3, CaCO3, BaSO4, ZnO, etc.) or hierarchical air pores; (4) to apply the modified organic polymer coatings on highly reflective metallic substrates.

It is worth mentioning that in 2021 Ruan et al.²² developed the whitest coating used the acrylic-based paint as the matrix and then modified it with highvolume BaSO₄ nanoparticles, achieving a solar reflectance of 98.1% and a sky window emissivity of 0.95. Applying this SDRCC onto a roof area of approximately 1000 square feet was said to be able to generate 10 kw of cooling power, making it an attractive alternative to air conditioning to cool buildings. A criticism on organic polymer coatings is that they originate mostly from

non-renewable fossil resources^{23,24} and their fabrication may be involved with the emission of volatile organic compounds (VOC), which generate a negative impact on human health and environment. In addition, the aging problems of organic materials are always a significant concern under various environmental and climatic conditions, such as UV radiation, elevated temperature, and moisture exposure as well as the fire.

Geopolymer is a new category of clinker-free (i.e., much reduced CO₂ emission during production) cementitious materials with three-dimensional inorganic alumino-silicate network, which is composed of silicon oxygen tetrahedron [SiO₄]⁴⁻ and aluminum oxygen tetrahedron [AlO₄] bridged by silicon-aluminum-oxygen bonds.²⁵ The high bond energies of the Si-O bond and the Al-O bond in the geopolymer structure make it hard to react with most acids at room temperature. Moreover, the dense nano-sized pores within the network lead to superior durability, chemical tolerance, and impermeability to other materials. Most importantly, the solar reflectance of metakaolin-based geopolymer itself is relatively high (over 70%), making it a good candidate for preparing the SDRCC, as illustrated in Figure 1.^{2,26}

This article aims to develop an environmentally friendly inorganic SDRCC based on geopolymer. The optical properties, including solar reflectance and infrared emissivity, of the geopolymer SDRCC were characterized. In addition, the durability, abrasion resistance, and water resistance of the developed coating were also tested to meet the relevant industrial standards of coatings.

2 **EXPERIMENTAL PROGRAM**

2.1 Raw materials

The inorganic geopolymer coating was made from metakaolin (i.e., the precursor material) and alkali activator (AA) solution which was prepared by mixing water, sodium hydroxide, and sodium silicate (with the molar ratio of 3.2 and solid content of 34.2%). The Venator BLANC FIXE N-type nano-precipitated barium sulfate (BaSO₄, 1 μm) and monodispersed silica nanosphere (nano-SiO₂, 99.5%, 30 \pm 5 nm) were used to improve the reflectance and infrared emission. The Polytetrafluoroethylene (PTFE DISP 33, fluoropolymer resin) was used as a lubricant additive to improve the film formability and calcium hydroxide powder (Ca[OH]2) in analytical grade was used to increase the early strength under ambient curing. Magnesium fluoride (MgF₂, AR, 3 µm, Sinopharm Chemical Reagent Co. Ltd.); barium titanite (BaTiO₃, AR, 200 nm RHAWN Chemical Co. Ltd.); lightweight lime (Light calcium carbonate, CaCO₃, AR, 1 μm;

Xilong Scientific Co., Ltd) and ground lime (Heavy cal-

cium carbonate, CaCO3, AR, 2 µm; Tianjin Kemiou Chemical Reagent Co., Ltd.) were selected for optical performance comparison. The modified silane coupling agent (KH-800, Hangzhou Jessica Chemical Co. Ltd.) was used for hydrophobic treatment of the developed coating for improving the waterproofing property and durability.

2.2 Synthesis of geopolymer coating

The alkali activator (AA) was prepared with the molar ratio (i.e., SiO₂/Na₂O) of 1.2 and solid content of 38.5%. About 50 g AA was firstly added to a beaker, and then 20 g MK and about 25 g Zirconium grinding beads were added into the beaker for mixing and stirring. During the stirring process, 20 g water, 3 g SiO₂, 70 g BaSO₄ and 10 g PTFE emulsion were added in order. The mixture was then stirred at 1200 rpm for 20 min. Afterwards, 1.5 g Ca(OH)₂ was added into the beaker with stirring for 2 min. The final product, alkali activated geopolymer (AAGP) slurry was then obtained by removing the Zirconium grinding beads through filtering. The coating was then sprayed onto a standard fiber cement board substrate with the dimensions of $300 \text{ mm} \times 300 \text{ mm} \times 4 \text{ mm}$, (GB/T 9271-2008) using a spray gun with pressure of 5 MPa for about 50 s and the operation was repeated in approximately 3 min. The thickness of the above coating film after drying was at 500 \pm 50 μ m as measured by a micrometer thickness gauge. Finally, the sample surface was treated with silane coupling agent KH-800 solution (diluted to 20% in ethanol) for hydrophobic treatment before field tests and durability tests.

2.3 **Optical measurements**

The solar absorbance, reflectance, and transmittance of the developed AAGP coatings were measured in accordance with ASTM E903-12, for which a PerkinElmer Lambda 1050+ UV/VIS/NIR Wide Band Spectrometer equipped with an integral sphere was employed. The infrared emissivity of AAGP coatings was measured using a FTIR spectrometer (Vertex 70, Bruker).

Material characterizations 2.4

To analyze the physicochemical properties of both raw materials (i.e., metakaolin, BaSO₄, nano silica, PTFE and Ca(OH)₂) and the formed AAGP coatings (i.e., with different fillers), XRD and FTIR analysis were conducted. XRD tests were performed to figure out the materials'

crystallographic structures on a Bruker D8 ADVANCE A25X X-ray Diffractometer (Bruker AXS Ltd., Germany); FTIR spectroscopy was tested on a Thermo Fisher Nicolet iS10 FTIR spectrophotometer (Thermo Fisher, Germany) to analyze the functional groups and corresponding characteristic peaks. To further identify the microstructural properties and elemental distributions in the AAGP cooling coating, SEM and EDS were examined using TESCAN VEGA3 (TESCAN ORSAY HOLDING, Kohoutovice, Brno). It should be noted that the optical tests were conducted for all the formed AAGP coatings while the other above-mentioned material characterization tests were conducted only for the AAGP coating with the optimal contents of BaSO₄ and SiO₂, which were respectively determined as 60 and 1.5 wt% based on the prior optical tests as discussed in the latter sessions.

2.5 | Field tests

To evaluate the cooling performance, the AAGP cooling coating was prepared on a standard fiber-reinforced cement board and then hydrophobically treated with silane coupling agent KH-800 for long-lasting maintenance of optimal properties. The real-time surface temperatures of uncoated board and AAGP coated boards were recorded using a multichannel temperature collec-(MEMORY HiLOGGER LR8431-30, HIOKI; E.E. Co. Ltd.). Thermocouple wires, KPS-TT-K-24-SLE-100 were purchased from Tianjin KAIPUSEN Heating & Cooling Equipment Co., Ltd. A mini weather station (Beijing Top Flag Technology Co., Ltd.) was installed for air temperature and humidity data collection.

2.6 | Durability tests

The linear abrasion test of AAGP coatings was carried out on standard sandpaper (320 mesh) with a 500 g abrading load²⁷ to compare the solar reflectance performance and microscopic appearance of the coating surface before and after the abrasion. Water permeability test of AAGP coating was carried out according to the standard of Japan Society of Civil Engineers JSCE-K571-2004. Pull-off tests of AAGP coatings were carried out with specially designed equipment (PosiTest® AT-M Adhesion Tester) according to the ASTM D4541. The size of the dolly used was 20 mm in diameter. All the above tests were carried out at room temperature. To determine the thermal stability and compositions of AAGP coating with different fillers, TGA tests were conducted on a Rigaku Thermo Plus EVO2 Thermalgravimetry Analyzer.

3 | RESULTS AND DISCUSSION

3.1 | Optical performance

In order to achieve high radiative cooling performance and daytime sub-ambient cooling, the coating needs to meet three conditions as follows²⁸:

- (1) minimizing the absorption from the solar spectrum (high solar reflectance).
- (2) maximizing the emissivity at the atmospheric window (high emittance in the wavelength of 8 to $13 \mu m$).

Similar to the previously reported strategies for boosting the solar reflectance and infrared emissivity of a polymeric coating, nano-sized functional fillers were utilized to modify the optical performance of AAGP coating. Nano-SiO₂ was chosen to improve the infrared emissivity. For solar spectrum, hierarchical air pores were formed in the geopolymer matrix and can introduce gentle light scattering. Moreover, other types of powders were added into the AAGP matrix to further facilitate multiple Mie scattering of sunlight (see Section 3.2.2). Semiconductors with large bandgap and high refractive index are favored for efficient scattering.

Figure 2A shows the measured solar reflectance of the formed AAGP geopolymer coatings modified with commonly used white wide band gap materials including BaSO₄, MgF₂, BaTiO₃, light-weight lime, and ground lime. To avoid agglomeration of BaTiO₃ powders and to avoid coagulation of light-weight lime, they were pre-treated with ethanol dissolved KH-800 silane coupling agent (the powders were immersed in KH-800 solution and then oven dried at 80°C for one hour). Table 1 summarizes the reflectance of different coatings integrated in different spectral regions (i.e., UV region, VIS region and NIR region) and the resultant overall reflectance. It can be observed that, comparing to other white materials, BaSO₄ enabled the AAGP coating with the highest reflectance in the UV range (0.8546) as well as a remarkable overall solar reflectance of 0.9690. Therefore, in spite of the difference existing between the polymeric and inorganic matrix, the dielectric contrast near geopolymer-air, geopolymer-BaSO₄ and air-BaSO₄ interfaces can efficiently introduce multiple Mie scattering and thus improve the overall solar reflectance, manifesting the similar mechanism to that observed in BaSO₄-modified polymeric cooling coatings.²⁹

Further research was conducted to investigate how the addition ratio of BaSO₄ in the AAGP matrix influences the solar reflectance the coating. Four different addition ratios of BaSO₄ varying from 50 to 70 w% were selected. It is shown that as the addition ratio of BaSO₄ increases, the solar reflectance of the AAGP coating

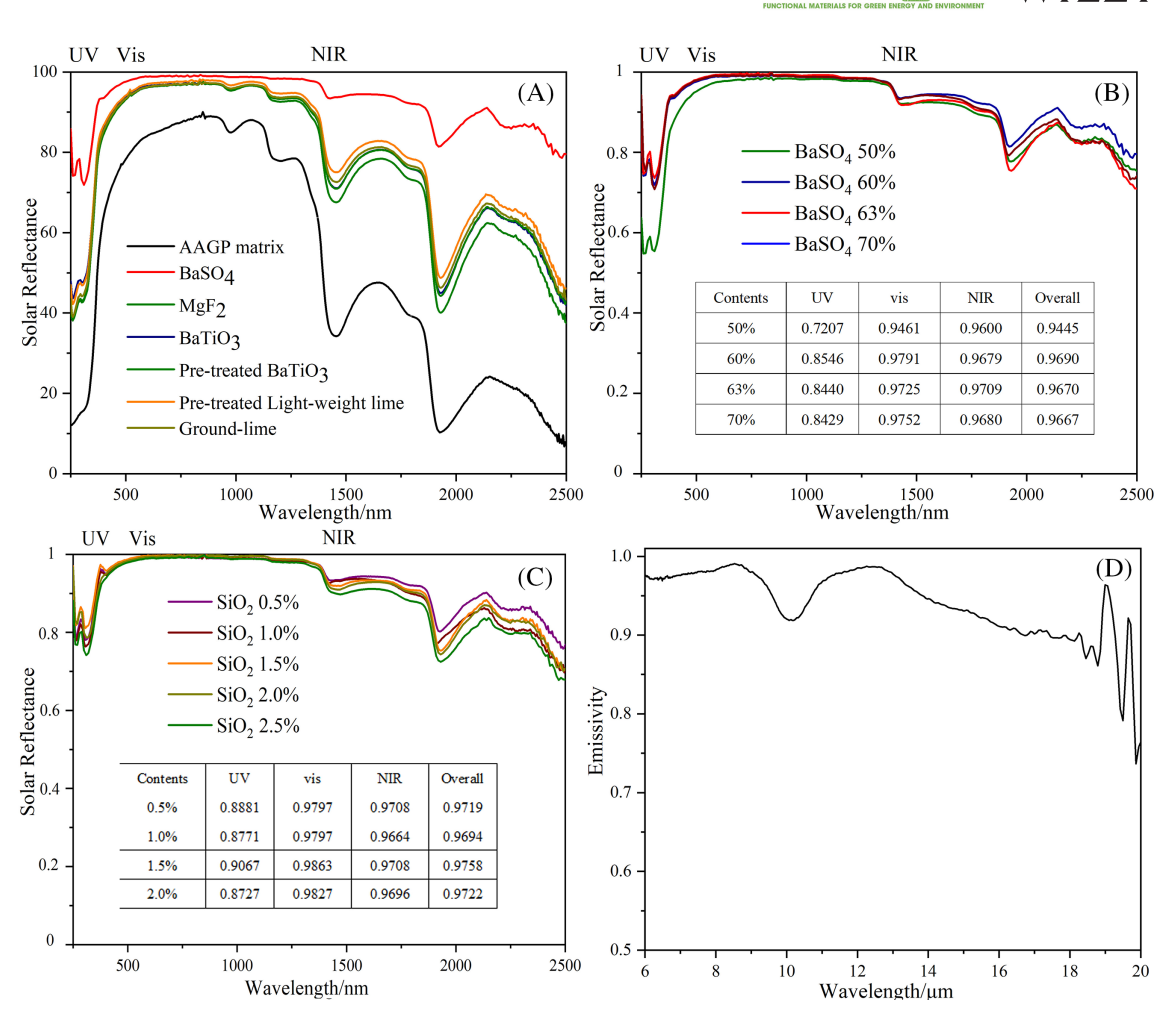


FIGURE 2 Optical properties of SDRCC samples with different functional fillers. (A) Solar reflectance of AAGP matrix and AAGP coatings with different fillers. (B, C) Solar reflectance of AAGP coatings with varied addition ratio of BaSO₄ (B) and further modification of SiO₂ (C). (D) Infrared emissivity of the optimized AAGP cooling coating

TABLE 1 Solar reflectance of AAGP coating with different additives in different spectral regions

Sample	UV	Vis	NIR	Overall
AAGP Matrix	0.3429	0.8076	0.7364	0.7620
AAGP Matrix with BaSO ₄	0.8546	0.9791	0.9679	0.9690
AAGP Matrix with BaTiO ₃	0.6694	0.9292	0.9023	0.9064
AAGP Matrix with pre-treated BaTiO ₃	0.6419	0.9238	0.9016	0.9025
AAGP Matrix with pre-treated light-weight lime	0.6716	0.9357	0.9165	0.9165
AAGP Matrix with ground lime	0.6511	0.9259	0.9058	0.9058

increases first and then decreases (see Figure 2B), with the maximum value overall reflectance reached at 60 wt% (i.e., 0.969). At the optimized addition ratio of $BaSO_4$ (i.e., 60 wt%), different amounts of $nano-SiO_2$ particles (0% to 2.5% of the matrix by weight) with high infrared emissivity were further added into the matrix to assist scattering. It is shown in Figure 2C that addition of 1.5 wt% $nano-SiO_2$ particles led to the best overall reflectance performance (i.e., 0.9758).

Figure 2D presents the measured spectral response of the thermal infrared (6–20 $\mu m)$ emissivity of the optimized AAGP cooling coating (i.e., with 60% BaSO4 and 1.5% SiO2). It is shown that the infrared emissivity both in and out of the sky window (8–13 $\mu m)$ was very high (0.9491). This high emissivity was attributed to the alumino-silicate network of geopolymer (-Si-O-Al[Si]-O-) as explained in the later sessions.

25673173, 2023. 2, Downloaded from https://onlinelibrary.wiley.com/doi/10.1002/com2.12284 by City University Of Hong Kong, Wiley Online Library on [23/11/2025]. See the Terms

conditions) on Wiley Online Library for rules of use; OA articles are governed by the applicable Creative Commons

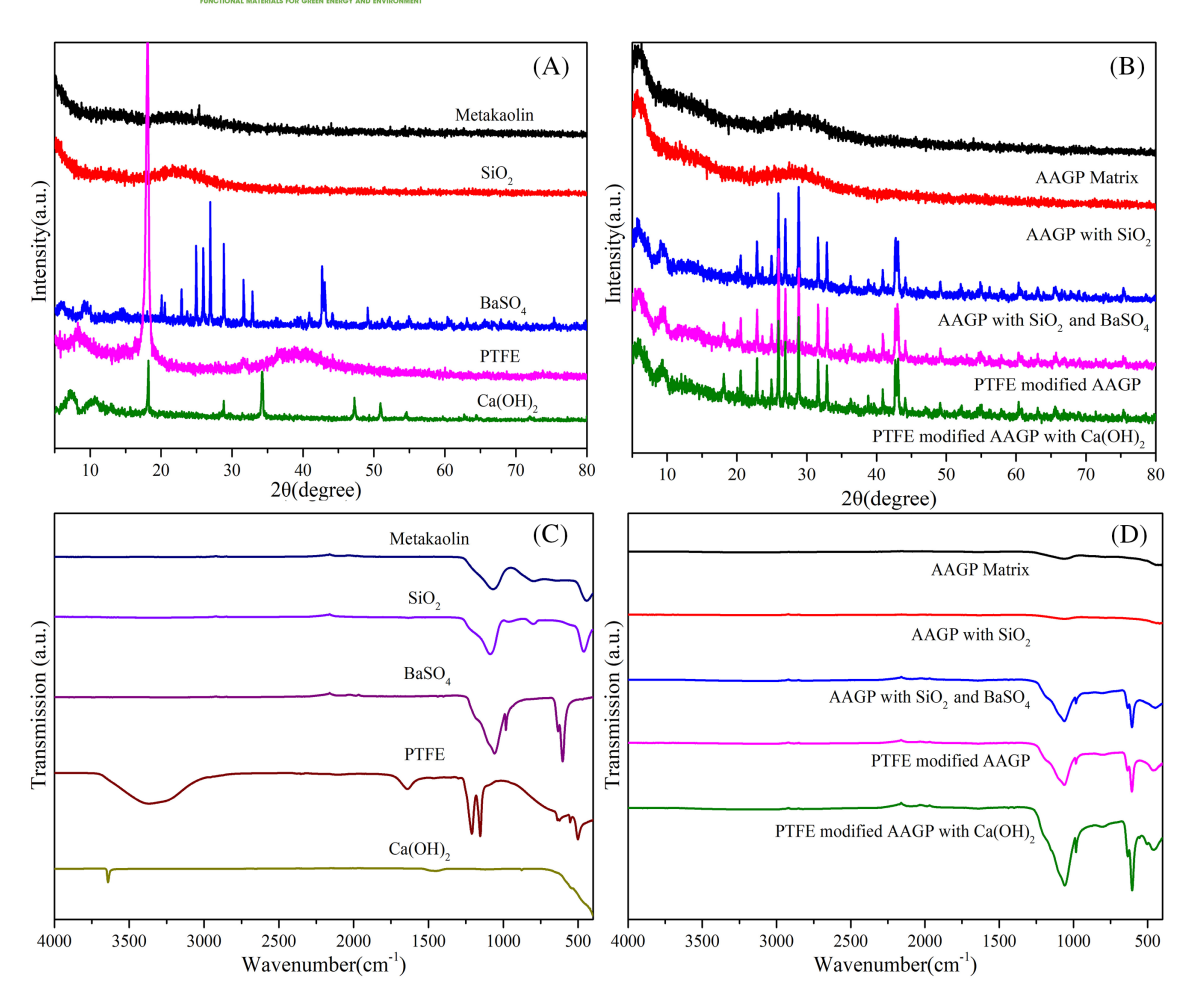


FIGURE 3 (A) XRD of the raw materials and (B) AAGP coatings with different fillers. FTIR of the raw materials (C), AAGP matrix and AAGP coatings with different fillers (D)

3.2 **Materials Characterizations**

3.2.1 XRD spectrum and FT-IR spectrum

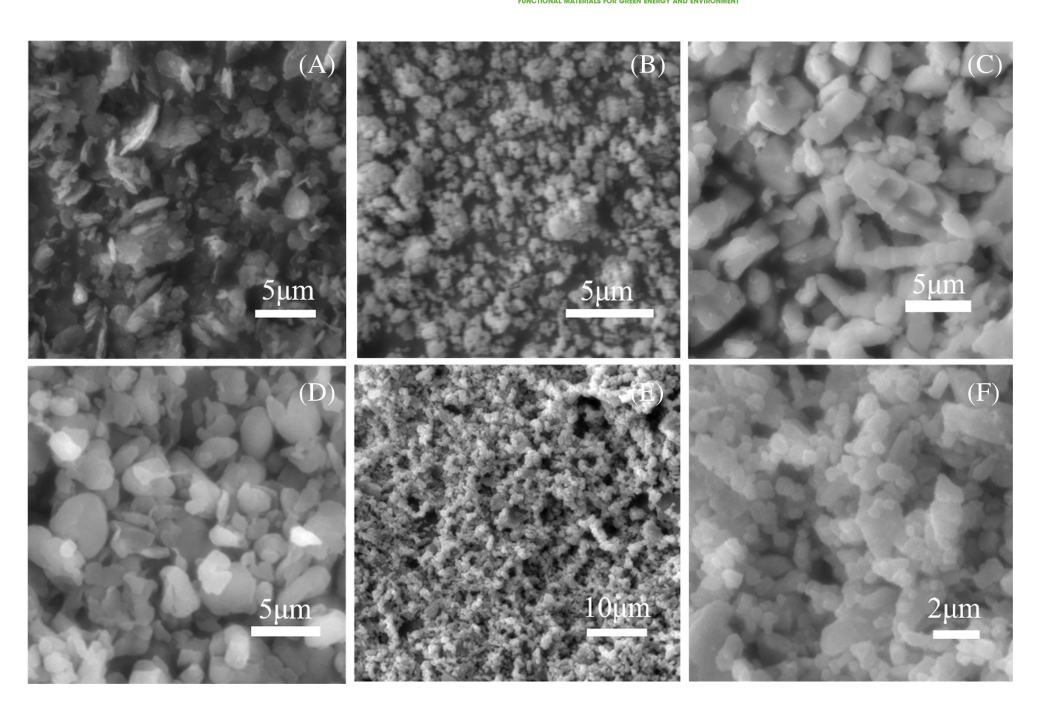
As shown in Figure 3A and B, the characteristic peaks of the raw materials of the coating and the changes in crystal structure after the coating formation were analyzed by XRD tests. The characteristic peaks of metakaolin include broad dispersion peaks with low intensity between 20° and 28.4°, indicating the mixed semi-crystalline and amorphous structure with strong reactivity, which facilitated the formation of geopolymer. The results show that the siloxane and aluminoxane tetrahedral structures in metakaolin disappeared to form three possible complex structural morphologies (-Al-O-Al-, -Si-O-Si-, or -Si-O-Al- chains), which are presented as phase shifts in Figure 3B.

The diffraction peaks of BaSO₄ are relatively sharp, indicating good crystallinity, high purity, and a hexagonal crystal structure (JCPDF file no. 24-1035). The characteristic peaks of BaSO4 can also be clearly observed

after being added into AAGP matrix, as shown in Figure 3B (blue line), which is a major function part of the cooling coating. The small amount of PTFE provided a small sharp characteristic peak at 18.5° (JCPDF file no. 54-1595) in the AAGP coating (pink line in Figure 3B). Addition of Ca(OH)₂ hardly changed the crystalline structure of the AAGP coating.

The functional groups of the raw materials and AAGP coating with different fillers were investigated through FTIR analysis, as shown in Figure 3C and D. The major characteristic peak of metakaolin locates at 1068 cm⁻¹ is in association with the Si-O asymmetric vibration. However, it shifts to 1060 cm⁻¹ in the geopolymer matrix, which can be attributed to the partial replacement of [SiO₄] tetrahedra by [AlO₄] tetrahedra that alters the local chemical environment of the Si-O bond. The characteristic bands centered at 798 and 777 cm⁻¹ in the metakaolin spectra are attributed to the stretching and bending vibrations of the six-coordinated Al-O, which is a highly reactive component of the metakaolin. These two peaks changed to one moderate peak at 784 cm⁻¹

FIGURE 4 SEM micrographs of metakaolin (A), SiO₂ (B), BaSO₄ (C), PTFE (D), and AAGP coatings under 2000× magnification (E) and 10 000× magnification (F)



after geopolymerization, which is the vibration of unit of the geopolymer structure Si-O-Al or Si-O-Si. The above intensive peaks (at 9.434 and 12.76 µm) in the infrared atmospheric window contributed to the high emissivity of the geopolymer matrix as discussed in the previous sessions. 27 The characteristic bands of BaSO₄ nanoparticle centered at 1060 cm⁻¹ and the shoulder at 984 cm⁻¹ were assigned to symmetric stretching vibration of SO₄ ²⁻ group. The peaks obtained at 637 and 603 cm⁻¹ were attributed to the out-of-plane bending vibration of the SO₄ ²⁻. As the BaSO₄ content exceeds half of the total content, most of the peaks of the AAGP cooling coating exhibited its characteristic peaks

3.2.2 SEM and element mapping results

The microscopic surface morphology of raw materials and AAGP coatings are shown in the Figure 4. It is seen that the three-dimensional geopolymer matrix formed the scaffold that bound up the BaSO₄ flakes and silica nanospheres, forming a surface morphology of intermingled micro-/nano- bulges and pores. Interestingly, hierarchical air pores were observed in the AAGP matrix, which is beneficial for enhancing solar reflectance.27,30

The element mapping of the coating surface was obtained by EDS analysis for which different colors vividly show the evenly distributed different chemical elements in the analyzed sample (Figure 5). The falsecolored SEM image shows that the fillers (purple color

for BaSO₄ and green color for SiO₂) and matrix (yellow) have been well mixed and evenly distributed.

3.3 Field cooling performance tests

The device (details are shown in Supplementary Note 1 and Figure S1) was placed on a flat building roof under direct sunlight on November 13, 2021, in Hong Kong, China. The relative humidity was recorded stably at around 40%. The average wind speed was 3 m s⁻¹. Figure 6A shows the variations of the ambient temperature and the surface temperatures of coated and uncoated cement boards within 24 h and Figure 6B shows the enlarged view during noon time (i.e., 11:00 a.m. to 1:00 p.m.). It is shown that the surface temperature of AAGP coating was consistently lower than the ambient temperature at daytime.

The detailed average temperature data of the uncoated board (T_{uc}) , AAGP coating (T_c) , and the ambient environment (T_a) are presented in Table 2. The results show that the AAGP coating could achieve an average temperature reduction of 4.09°C and a maximum temperature reduction of 8.9°C compared to the ambient (i.e., T_a-T_c), while the average and maximum temperature differences between AAGP coated and uncoated boards (i.e., $T_{\rm uc}-T_{\rm c}$) were 5.54°C and 24.30°C, respectively.

In addition, our AAGP coating exhibited excellent durability under abrasion, water permeation, and high temperatures as well as an excellent bonding performance (see Supplementary Notes 2-4), indicating it is a

25673173, 2023, 2, Downloaded from https://onlinelibrary.wiley.com/doi/10.1002/eom2.12284 by City University Of Hong Kong, Wiley Online Library on [23/11/2025]. See the Terms

conditions) on Wiley Online Library for rules of use; OA articles are governed by the applicable Creative Commons License

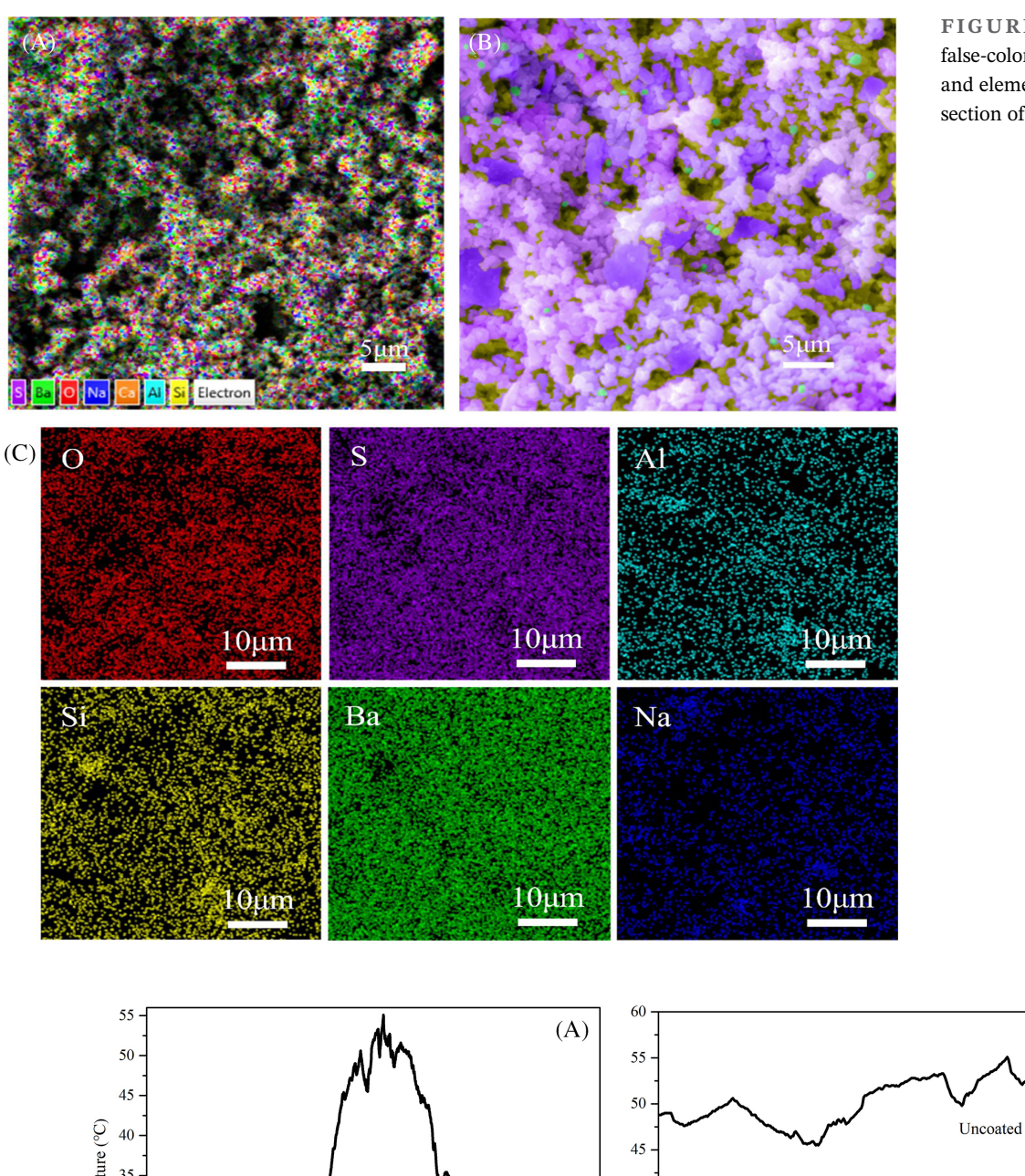


FIGURE 5 SEM image (A), false-colored SEM image (B), and elemental mapping (C) of section of the AAGP coating

(B) Temperature (°C) Uncoated Board 35 40 30 35 25 30 20 25 15 AAGP coated Board 10 04:00 08:00 12:00 16:00 20:00 24:00 13:00 00:00 12:00 12:30 11:00 11:30 Time of day (24 hours) Time of day (at noon)

FIGURE 6 Cooling performance of an AAGP-coated board in comparison to an uncoated board

Average (°C) temperature	$T_{ m uc}$	T_{c}	T_{a}	$T_{\rm a}-T_{\rm c}$	$T_{ m uc}{-}T_{ m c}$
11 a.m. to 1 p.m.	32.79	22.07	25.77	3.70	10.72
12 a.m. to 12 p.m.	25.25	19.71	23.80	4.09	5.54

TABLE 2 Average temperatures of uncoated board and AAGP-coated board

superior alternative for long-term large-scale applications of radiative cooling coatings.

4 | CONCLUSIONS

An inorganic geopolymer-based daytime radiative cooling coating has been developed in this study, which is environment-friendly and can be formed and cured at room temperature. Based on a comprehensive experimental study program, the following conclusions have been arrived:

- The AAGP coating has achieved a high sky window emissivity of 0.9491 and 97.6% of solar reflectance mainly due to the addition of BaSO₄ and nano-SiO₂ particles and the hierarchical air pores formed in the AAGP matrix.
- 2. The optimized AAGP coating could achieve a subambient cooling effect up to 8.9 °C under direct sunlight.
- The developed AAGP coating could maintain well its performance after mechanical wearing and high temperature exposure and exhibit good waterproofing resistance.

Due to the inherit advantages of an inorganic coating over its organic counterpart, the developed AAGP coating is expected to be able to broaden the applicability of the SDRC technology for efficient thermal management and energy saving purpose.

ACKNOWLEDGMENTS

We acknowledge the financial support by RGC General Research Fund (Project No. 15223120), Research Institute for Sustainable Urban Development (Project No. 1-BBWX) and Research Institute for Smart Energy (Project No. CDBL) of The Hong Kong Polytechnic University. The first author would like to thank the PhD studentship provided the Hong Kong Polytechnic University.

CONFLICT OF INTEREST

The authors declare no conflict of interest.

ORCID

Dangyuan Lei https://orcid.org/0000-0002-8963-0193 Jian-Guo Dai https://orcid.org/0000-0001-9904-7914

REFERENCES

1. Vacquier V. The measurement of thermal conductivity of solids with a transient linear heat source on the plane surface of a

- poorly conducting body. *Earth Planet Sci Lett.* 1985;74(2–3): 275-279. doi:10.1016/0012-821X(85)90027-5
- 2. Zhao B, Hu M, Ao X, Chen N, Pei G. Radiative cooling: a review of fundamentals, materials, applications, and prospects. *Appl Energy*. 2019;236:489-513. doi:10.1016/j.apenergy.2018. 12.018
- 3. Ahmed S, Li Z, Javed MS, Ma T. A review on the integration of radiative cooling and solar energy harvesting. *Materials Today Energy*. 2021;21:100776. doi:10.1016/j.mtener.2021.100776
- Zhao B, Hu M, Ao X, Xuan Q, Pei G. Spectrally selective approaches for passive cooling of solar cells: a review. *Appl Energy*. 2020;262:114548. doi:10.1016/j.apenergy.2020.114548
- Raman AP, Anoma MA, Zhu L, Rephaeli E, Fan S. Passive radiative cooling below ambient air temperature under direct sunlight. *Nature*. 2014;515(7528):540-544. doi:10.1038/ nature13883
- Fan S, Li W. Photonics and thermodynamics concepts in radiative cooling. *Nature Photonics*. 2022;16(3):182-190. doi:10.1038/s41566-021-00921-9
- 7. Ko B, Lee D, Badloe T, Rho J. Metamaterial-based radiative cooling: towards energy-free all-day cooling. *Energies*. 2018; 12(1):89. doi:10.3390/en12010089
- Said Z, Arora S, Farooq S, Sundar LS, Li C, Allouhi A. Recent advances on improved optical, thermal, and radiative characteristics of plasmonic nanofluids: academic insights and perspectives. Sol Energy Mater Sol Cells. 2022;236:111504. doi:10. 1016/j.solmat.2021.111504
- 9. Lee D, Go M, Son S, et al. Sub-ambient daytime radiative cooling by silica-coated porous anodic aluminum oxide. *Nano Energy*. 2021;79:105426. doi:10.1016/j.nanoen.2020.105426
- Son S, Liu Y, Chae D, Lee H. Cross-linked porous polymeric coating without a metal-reflective layer for sub-ambient radiative cooling. ACS Appl Mater Interfaces. 2020;12(52):57832-57839. doi:10.1021/acsami.0c14792
- 11. Kim M, Lee D, Son S, Yang Y, Lee H, Rho J. Visibly transparent radiative cooler under direct sunlight. *Advanced Optical Materials*. 2021;9(13):2002226. doi:10.1002/adom.202002226
- 12. Zhai Y, Ma Y, David SN, et al. Scalable-manufactured randomized glass-polymer hybrid metamaterial for daytime radiative cooling. *Science*. 2017;355(6329):1062-1066. doi:10.1126/science.aai7899
- Xue C-H, Wei R-X, Guo X-J, et al. Fabrication of superhydrophobic P(VDF-HFP)/SiO2 composite film for stable radiative cooling. *Compos Sci Technol*. 2022;220:109279. doi:10.1016/j. compscitech.2022.109279
- Liu J, Tang H, Zhang J, Zhang D, Jiao S, Zhou Z. Boosting daytime radiative cooling performance with nanoporous polyethylene film. *Energy and Built Environment*. 2021. doi:10.1016/j. enbenv.2021.10.001
- Chen M, Pang D, Chen X, Yan H. Enhancing infrared emission behavior of polymer coatings for radiative cooling applications. J Phys D Appl Phys. 2021;54(29):295501. doi:10.1088/1361-6463/abfb19
- Huang J, Fan D, Li Q. Structural rod-like particles for highly efficient radiative cooling. *Materials Today Energy*. 2022; 100955.
- 17. Cui J, Li XQ, Pei ZQ, Pei YS. A long-term stable and environmental friendly self-healing coating with polyaniline/sodium alginate microcapsule structure for corrosion protection of



- water-delivery pipelines. *Chem Eng J.* 2019;358:379-388. doi:10. 1016/j.cej.2018.10.062
- Yuan J, Yin H, Yuan D, Yang Y, Xu S. On daytime radiative cooling using spectrally selective metamaterial based building envelopes. *Energy*. 2022;242:122779. doi:10.1016/j.energy.2021. 122779
- 19. Li J, Liang Y, Li W, et al. Protecting ice from melting under sunlight via radiative cooling. *Sci Adv.* 2022;8(6):eabj9756.
- 20. Zhou K, Li W, Patel BB, et al. Three-dimensional printable nanoporous polymer matrix composites for daytime radiative cooling. *Nano Lett.* 2021;21(3):1493-1499. doi:10.1021/acs. nanolett.0c04810
- Mandal J, Fu Y, Overvig AC, et al. Hierarchically porous polymer coatings for highly efficient passive daytime radiative cooling. *Science*. 2018;362(6412):315-319. doi:10.1126/science. aat9513
- Li XY, Peoples J, Yao PY, Ruan XL. Ultrawhite BaSO4 paints and films for remarkable daytime subambient radiative cooling. ACS Appl Mater Interfaces. 2021;13(18):21733-21739. doi: 10.1021/acsami.1c02368
- Y-1 S, Darani KS, Khdair AI, Abu-Rumman G, Kalbasi R. A review on conventional passive cooling methods applicable to arid and warm climates considering economic cost and efficiency analysis in resource-based cities. *Energy Rep.* 2021;7: 2784-2820. doi:10.1016/j.egyr.2021.04.056
- Liu J, Zhou Z, Zhang J, Feng W, Zuo J. Advances and challenges in commercializing radiative cooling. *Materials Today Physics*. 2019;11:100161. doi:10.1016/j.mtphys.2019.100161
- Wang YS, Alrefaei Y, Dai JG. Silico-aluminophosphate and alkali-aluminosilicate Geopolymers: a comparative review. Frontiers in Materials. 2019;6:106. doi:10.3389/fmats.2019. 00106

- 26. Chen J, Lu L. Development of radiative cooling and its integration with buildings: a comprehensive review. *Solar Energy*. 2020;212:125-151. doi:10.1016/j.solener.2020.10.013
- 27. Chen G, Wang Y, Qiu J, et al. Robust inorganic daytime radiative cooling coating based on a phosphate Geopolymer. *ACS Appl Mater Interfaces*. 2020;12(49):54963-54971. doi:10.1021/acsami.0c15799
- 28. Sun J, Wang J, Guo T, Bao H, Bai S. Daytime passive radiative cooling materials based on disordered media: a review. *Sol Energy Mater sol Cells.* 2022;236:111492. doi:10.1016/j.solmat. 2021.111492
- 29. Xue X, Qiu M, Li YW, et al. Creating an eco-friendly building coating with smart subambient radiative cooling. *Adv Mater*. 2020;32(42). doi:10.1002/adma.201906751
- Li D, Liu X, Li W, et al. Scalable and hierarchically designed polymer film as a selective thermal emitter for highperformance all-day radiative cooling. *Nat Nanotechnol*. 2021; 16(2):153-158. doi:10.1038/s41565-020-00800-4

SUPPORTING INFORMATION

Additional supporting information can be found online in the Supporting Information section at the end of this article.

How to cite this article: Yang N, Fu Y, Xue X, Lei D, Dai J-G. Geopolymer-based sub-ambient daytime radiative cooling coating. *EcoMat.* 2023; 5(2):e12284. doi:10.1002/eom2.12284